



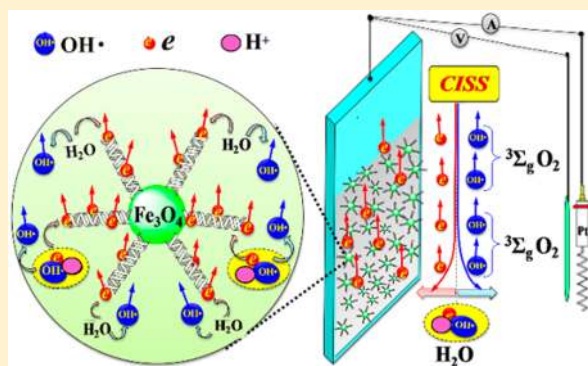
# Enhanced Electrochemical Water Splitting with Chiral Molecule-Coated $\text{Fe}_3\text{O}_4$ Nanoparticles

Wenyan Zhang, Koyel Banerjee-Ghosh, Francesco Tassinari, and Ron Naaman\*

Department of Chemical and Biological Physics, Weizmann Institute of Science, Rehovot 76100, Israel

 Supporting Information

**ABSTRACT:** Photoelectrochemical (PEC) water splitting is a promising approach for generating hydrogen from water. In order to enhance PEC water splitting efficiency, it is essential to inhibit the production of the hydrogen peroxide byproduct and to reduce the overpotential required by an inexpensive catalyst and with high current density. In the past, it was shown that coating  $\text{TiO}_2$  electrodes by chiral molecules or chiral films enhances the hydrogen production and reduces the production of  $\text{H}_2\text{O}_2$  byproduct. This was explained to be a result of the chiral-induced spin selectivity (CISS) effect that induces spin correlation between the electrons transferred to the anode. However, typically the current observed in those studies was in the range of 1–100  $\mu\text{A}/\text{cm}^2$ . Here we report currents in the range of 10  $\text{mA}/\text{cm}^2$  obtained by adsorbing chiral molecules on a well-established  $\text{Fe}_3\text{O}_4$  nanoparticle (NP) catalyst deposited on the anode. The results indicate a new strategy for designing low-cost earth-abundant catalysts where the advantages of the CISS effect are combined with the large effective area provided by the NPs to promote PEC water splitting with high current density.



For decades, alternative energy research has focused on attempting to produce hydrogen efficiently by splitting water in a photoelectrochemical (PEC) process.<sup>1–6</sup> Despite the impressive progress made over the years,<sup>7</sup> the obtained properties are still below what is considered sufficient for practical applications.<sup>1–3,6</sup> Three main obstacles currently exist in order to make PEC processes practical. The first is the overpotential required, which is typically about 0.6 V above the thermodynamic minimum potential of 1.23 V. The second is the production of the hydrogen peroxide byproduct, which poisons the electrodes, reduces the anodes' current, and shortens their lifetime.<sup>8–10</sup> The third obstacle is the relatively low current densities obtained.

Recently, we found experimentally that the  $\text{H}_2\text{O}_2$  production, the overpotential, and the anode current are correlated and can be modified by controlling the spin of the electrons injected into the anode. It has been proposed that this spin control produces spin alignment in the unpaired electrons of the intermediate radicals ( $\cdot\text{OH}$ ) that combine to form the ground-state triplet oxygen molecule ( $^3\text{O}_2$ ). This model also rationalizes the suppressed production of hydrogen peroxide, which is a singlet species and therefore cannot be formed by combining OH radicals because the spins of their unpaired electrons are aligned parallel to each other.<sup>11–14</sup> Hence, polarizing the spin of  $\cdot\text{OH}$  prevents  $\text{H}_2\text{O}_2$  evolution

and reduces the overpotential. The spin control in the PEC process was achieved by applying the chiral-induced spin selectivity (CISS) effect, which allows spin selectivity in electrons transferred through chiral molecules.<sup>15–17</sup> In previous studies, the  $\text{TiO}_2$  anode was coated with a monolayer of chiral molecules or with a chiral film to achieve the spin selectivity. However, those studies failed to achieve high anode currents and usually the current density obtained was below 1  $\text{mA}/\text{cm}^2$ , as is often found for anodes coated with organic molecules.<sup>18</sup>

Here, we report the application of the CISS effect with a well-established and efficient catalyst in order to enhance the anode current, to suppress hydrogen peroxide production, and to reduce the overpotential for PEC water splitting. Chiral molecules were chemisorbed on  $\text{Fe}_3\text{O}_4$  nanoparticles (NPs) that were deposited on a (fluorine-doped tin oxide) FTO anode. The  $\text{Fe}_3\text{O}_4$  NPs are smaller than 20 nm and therefore exhibit large surface areas and abundant reactive sites on the anode. In addition, the chiral molecules induce chirality in the NPs, and as a result, the electron transfer from a solution to an anode is spin-selective, and therefore, the formation of  $\text{H}_2\text{O}_2$  is

Received: August 9, 2018

Accepted: September 4, 2018

Published: September 4, 2018

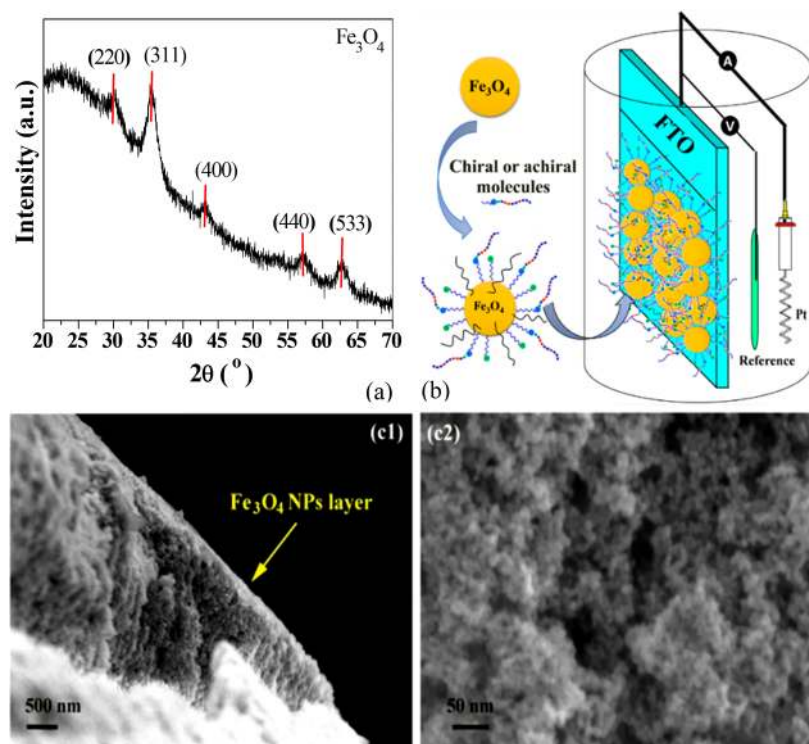


Figure 1. (a) XRD pattern of  $\text{Fe}_3\text{O}_4$  NPs; (b) scheme for assembling chiral and achiral molecules on  $\text{Fe}_3\text{O}_4$  NPs and coating the chiral and achiral  $\text{Fe}_3\text{O}_4$  NPs on the surface of FTO glass as an anode for water splitting; (c1) SEM images of an  $\text{Fe}_3\text{O}_4$  layer deposited on FTO glass, cross-view; (c2) SEM images of  $\text{Fe}_3\text{O}_4$  (NPs), top-view.

suppressed and the triplet oxygen evolution is enhanced. Compared with an achiral anode, an anode coated with chiral  $\text{Fe}_3\text{O}_4$  NPs exhibits larger current density while being stable.

An X-ray diffraction pattern of the  $\text{Fe}_3\text{O}_4$  NPs is shown in Figure 1a. The diffraction peaks could be indexed to the (220), (311), (400), (440), and (533) planes of cubic  $\text{Fe}_3\text{O}_4$  (JCPDS# 65-3107). To investigate the CISS effect, the  $\text{Fe}_3\text{O}_4$  NPs were coated with four kinds of chiral molecules: L-tryptophan, D-tryptophan, L-A3, and L-A11 (see Table 1), as well as two kinds of achiral molecules: MPA and AIB<sub>10</sub> (see Table 1). These NPs are respectively denoted as  $\text{Fe}_3\text{O}_4$ @L-tryptophan,  $\text{Fe}_3\text{O}_4$ @D-tryptophan,  $\text{Fe}_3\text{O}_4$ @L-A3,  $\text{Fe}_3\text{O}_4$ @L-A11,  $\text{Fe}_3\text{O}_4$ @MPA, and  $\text{Fe}_3\text{O}_4$ @AIB<sub>10</sub>. They were coated on the surface of FTO glass that was used as the anode for the water splitting reaction, as schematically shown in Figure 1b. Figure 1c1 shows that the thickness of the  $\text{Fe}_3\text{O}_4$  layer is about 2  $\mu\text{m}$ .

The prepared  $\text{Fe}_3\text{O}_4$ NPs are smaller than 20 nm (Figures 1c2 and S2). It is known that the surface area and surface energy increase vastly when the NP's size decreases.<sup>19,20</sup>

Figure 2 presents the absorption and the circular dichroism (CD) spectra of the  $\text{Fe}_3\text{O}_4$ @L-A3 NPs. As is well-known, the  $\text{Fe}_3\text{O}_4$  NPs absorb almost continuously through the visible region of the spectrum; hence, they are ideal for a solar-based PEC device (Figure 2a). The CD spectrum provides an interesting indication of the chiral molecule-induced chirality in the NPs themselves. As shown in Figure 2b, the chiral L-A3 molecules exhibited two CD peaks at 201 and 226 nm, which stem from the  $\alpha$ -helix conformation of L-A3 chains. Attaching L-A3 to  $\text{Fe}_3\text{O}_4$  results in a CD spectrum in the range of the  $\text{Fe}_3\text{O}_4$  NPs' absorption. This effect of induced chirality in NPs, as a result of the adsorption of chiral molecules, is well documented for both metal and semiconducting NPs<sup>21–23</sup> and

Table 1. Chiral and Achiral Molecules Used

Chiral molecules	Molecular formula	Structural scheme
D-tryptophan	$\text{C}_{11}\text{H}_{12}\text{N}_2\text{O}_2$	
L-Tryptophan	$\text{C}_{11}\text{H}_{12}\text{N}_2\text{O}_2$	
L-A3	$\text{SH}-(\text{CH}_2)_2-\text{NH}-(\text{Ala}-\text{Aib})_3-\text{COOH}$	
L-A11	$\text{SH}-(\text{CH}_2)_2-\text{NH}-(\text{Ala}-\text{Aib})_{11}-\text{NH}_2$	
Achiral molecules	Molecular formula	Structural scheme
MPA	$\text{SH}-(\text{CH}_2)_2-\text{COOH}$	
AIB <sub>10</sub>	$\text{SH}-(\text{CH}_2)_2-\text{NH}-(\text{Aib})_{10}-\text{NH}_2$	

is demonstrated here for the  $\text{Fe}_3\text{O}_4$  NPs.<sup>24,25</sup> It was observed for all chiral molecules studied in the present work. In the past, it has been shown that electron transfer through semiconducting NPs coated with chiral molecules is spin-dependent.<sup>26</sup>

The catalytic activities of different anodes were evaluated by comparing their electrochemical performance in water splitting. As shown in Figure 3a–c, under a voltage of 1.23

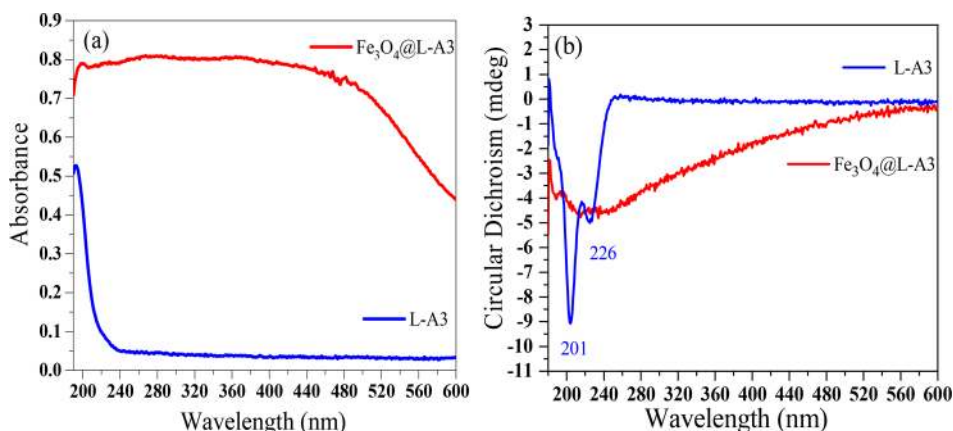


Figure 2. (a) Absorption spectra of a 1 mM L-A3 solution (blue line) and Fe<sub>3</sub>O<sub>4</sub>@L-A3 (red line); (b) CD spectra of a 1 mM L-A3 (blue line) solution and Fe<sub>3</sub>O<sub>4</sub>@L-A3 (red line).

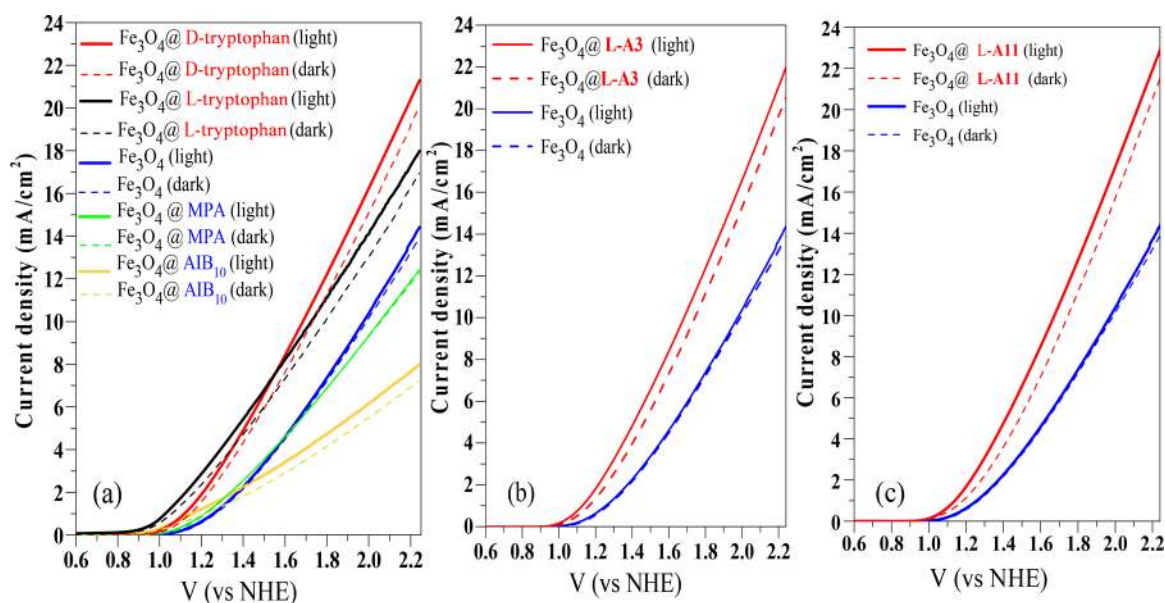


Figure 3. Photocurrent density (marked as light) and dark current density (marked as dark) of different samples (applied potential plots with respect to the normal hydrogen electrode (NHE)). The photocurrent was measured under visible light irradiation (power 8 W), and dark current was detected without light irradiation. Electrochemical measurements were conducted with a 0.1 M KOH solution (pH 13) as the electrolyte solution, with a scanning speed of 20 mV/s, and with a saturated calomel electrode as a reference.  $E(\text{NHE}) = E(\text{vs calomel}) + E^\circ(\text{calomel})$ , where  $E^\circ(\text{calomel}) = 0.241 \text{ V}$ . (a) Photocurrent density (light) and dark current density (dark) of Fe<sub>3</sub>O<sub>4</sub> NPs linked to D-tryptophan (chiral), Fe<sub>3</sub>O<sub>4</sub> NPs linked to L-tryptophan (chiral), Fe<sub>3</sub>O<sub>4</sub> NPs linked to MPA (3-mercaptopropionic acid, achiral), pure Fe<sub>3</sub>O<sub>4</sub> NPs, and Fe<sub>3</sub>O<sub>4</sub> NPs linked to AIB<sub>10</sub> (NH-(CH<sub>2</sub>)<sub>2</sub>-SH-(AIB)<sub>10</sub>-NH<sub>2</sub>, achiral); (b) Fe<sub>3</sub>O<sub>4</sub> NPs linked to L-A3 (SH-(CH<sub>2</sub>)<sub>2</sub>-NH-(Ala-AIB)<sub>3</sub>-COOH, chiral) and pure Fe<sub>3</sub>O<sub>4</sub> NPs; (c) Fe<sub>3</sub>O<sub>4</sub> NPs linked to L-A11 (SH-(CH<sub>2</sub>)<sub>2</sub>-NH-(Ala-AIB)<sub>11</sub>-NH<sub>2</sub>, chiral) and pure Fe<sub>3</sub>O<sub>4</sub> NPs.

V (vs NHE), the anode currents of Fe<sub>3</sub>O<sub>4</sub>@L-tryptophan, Fe<sub>3</sub>O<sub>4</sub>@D-tryptophan, Fe<sub>3</sub>O<sub>4</sub>@L-A3, and Fe<sub>3</sub>O<sub>4</sub>@L-A11 are, respectively, 3.5, 3.1, 3.0, and 2.7 times higher than that of pristine Fe<sub>3</sub>O<sub>4</sub> NPs. In addition, the anode currents of Fe<sub>3</sub>O<sub>4</sub> NPs coated with chiral molecules are much larger than those for Fe<sub>3</sub>O<sub>4</sub> NPs linked to achiral molecules of MPA and AIB. These results provide strong evidence that chiral molecules play a significant role in enhancing anode currents for water splitting. As expected, there is no difference regarding the activity of L or D enantiomers because in both cases the electrons' transfer is spin-selective and the main parameter is the correlation of the spin alignment among the electrons and not the specific direction of the spins in the laboratory frame.

Another interesting behavior characterizing Fe<sub>3</sub>O<sub>4</sub>@L-tryptophan, Fe<sub>3</sub>O<sub>4</sub>@D-tryptophan, Fe<sub>3</sub>O<sub>4</sub>@L-A3, and

Fe<sub>3</sub>O<sub>4</sub>@L-A11 is their sensitive response to light illumination. As shown in Figure 3a–c, the anode current of these four anodes increases under visible light irradiation of an LED lamp, which has quite low power (8 W). Meanwhile, a stability study showed that the chiral NPs coated on the anode have robust catalytic performance for splitting water, as seen in Figure S3.

To verify the role of the CISS effect in this process, we investigated the formation of hydrogen peroxide during the water splitting reaction using anodes coated with different NPs. In these studies, *o*-tolidine was used as a redox indicator for the presence of H<sub>2</sub>O<sub>2</sub>. The reaction was carried on in a 0.1 M Na<sub>2</sub>SO<sub>4</sub> electrolyte solution by applying a potential of 2.04 V vs NHE for 2 h.<sup>27,28</sup> When H<sub>2</sub>O<sub>2</sub> is present, a yellow color appears with an absorption peak at about 436 nm due to the oxidative reaction of *o*-tolidine with H<sub>2</sub>O<sub>2</sub>. As shown in Figure

4, a large absorption peak appeared at 436 nm when the anode was coated by achiral  $\text{Fe}_3\text{O}_4$  NPs, namely, the  $\text{Fe}_3\text{O}_4$ @MPA

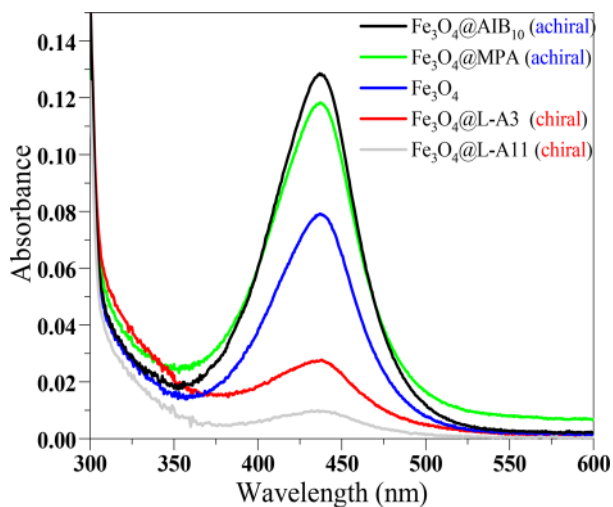


**Figure 4.** Visible absorption spectra from titration of the electrolyte used (0.1 M  $\text{Na}_2\text{SO}_4$ ) with *o*-tolidine of bare  $\text{Fe}_3\text{O}_4$ ,  $\text{Fe}_3\text{O}_4$ @L-A11 (chiral),  $\text{Fe}_3\text{O}_4$ @L-A3 (chiral),  $\text{Fe}_3\text{O}_4$ @MPA (achiral), and  $\text{Fe}_3\text{O}_4$ @AIB<sub>10</sub> (achiral).

NPs and  $\text{Fe}_3\text{O}_4$ @AIB<sub>10</sub>NPs. Only a very small peak appeared at 436 nm when the chiral  $\text{Fe}_3\text{O}_4$  NPs ( $\text{Fe}_3\text{O}_4$ @L-A11 and  $\text{Fe}_3\text{O}_4$ @L-A3) were used on the anode. This result provides strong evidence that chiral  $\text{Fe}_3\text{O}_4$ @L-A11 and  $\text{Fe}_3\text{O}_4$ @L-A3 NPs play a significant role in inhibiting the formation of  $\text{H}_2\text{O}_2$ . Moreover, Figure 4 shows that, compared with  $\text{Fe}_3\text{O}_4$ @L-A3, L-A11 exhibited better performance in suppressing the production of  $\text{H}_2\text{O}_2$ . This phenomenon demonstrates that the L-A11 molecules have a stronger CISS effect than the L-A3 molecules. Their longer chains induce higher spin selectivity.<sup>15,16</sup>

Compared with achiral  $\text{Fe}_3\text{O}_4$  NPs, the chiral ones show a CD response, larger anode currents, and low  $\text{H}_2\text{O}_2$  production. Therefore, we can conclude that the CISS effect plays a significant role in enhancing water splitting efficiency. Namely,

when the electrons are transferred from  $\text{OH}^-/\text{H}_2\text{O}$  to the anode, the chiral  $\text{Fe}_3\text{O}_4$  NPs filter them, so that only one spin state can be transferred to all electrons. This ensures that all newly generated  $\cdot\text{OH}$  radicals are left with their spins aligned parallel to each other. Those parallel-aligned  $\cdot\text{OH}$  radicals interact on the triplet potential surface to form ground-state oxygen molecules ( ${}^3\Sigma_g({}^3\text{O}_2)$ ), as illustrated in Figure 5a2). Here, it should be noted that  $\text{H}_2\text{O}_2$  will not be produced together with  ${}^3\text{O}_2$ , because the formation of  $\text{H}_2\text{O}_2$  is spin-forbidden on the triplet potential surface.

In contrast, when  $\text{Fe}_3\text{O}_4$  NPs are linked to achiral molecules (like MPA and AIB<sub>10</sub>), they do not filter the spin state of electrons; thus, the newly generated  $\cdot\text{OH}$  radicals are formed with randomly oriented spins, some of which are aligned antiparallel to each other. The antiparallel-aligned  $\cdot\text{OH}$  radicals interact on the singlet potential surface, leading to the formation of singlet hydrogen peroxide or singlet-state oxygen ( ${}^1\Delta_g({}^1\text{O}_2)$ , Figure 5a1), which lies about 1 eV above the triplet ground state (Figure 5b). The overpotential observed is a result of the system developing on the singlet potential energy surface to the point that intersystem crossing occurs and the system switches to the triplet surface. The energy at which the intersystem crossing takes place is below the energy corresponding to the  ${}^1\text{O}_2$  formation but is above the energy required for the formation of the singlet hydrogen peroxide. Hence, oxidation of water to  $\text{O}_2$ , when occurring without spin restriction, results in a large overpotential and the formation of kinetically favorable  $\text{H}_2\text{O}_2$  (Figure 5c). The newly produced  $\text{H}_2\text{O}_2$  may be adsorbed on the electrodes and poison them, thus resulting in a low anode current and poor catalytic stability for water splitting.

In summary, chiral  $\text{Fe}_3\text{O}_4$  NPs were synthesized by utilizing adsorbed chiral molecules to induce their chirality. In a PEC water splitting cell, the spin filtering properties of the chiral  $\text{Fe}_3\text{O}_4$  NPs induces spin alignment of electrons in the generated hydroxyl radicals, thus effectively inhibiting the formation of hydrogen peroxide while promoting the production of triplet oxygen. Owing to the CISS effect, the large surface area, and the abundant reactive sites, the anode coated with chiral  $\text{Fe}_3\text{O}_4$  NPs exhibits large currents of

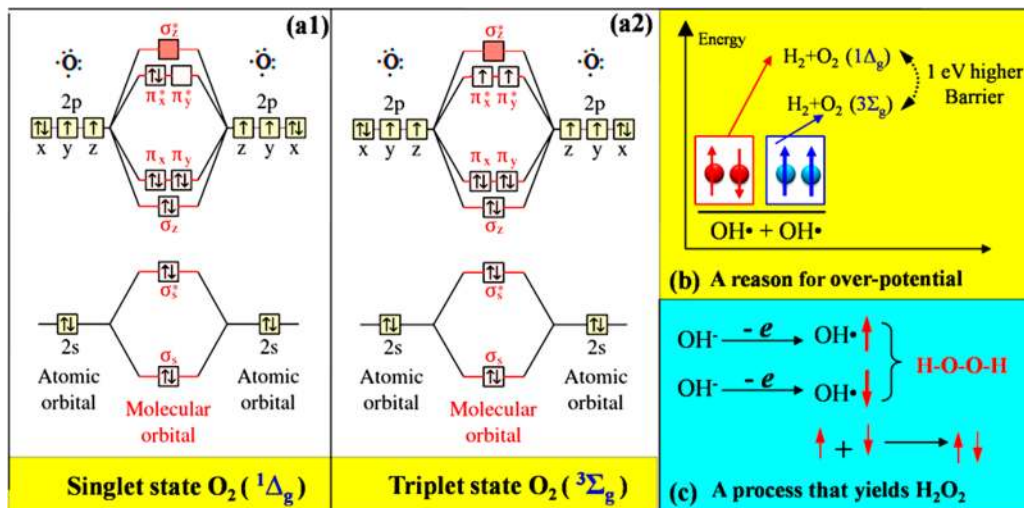


**Figure 5.** (a1) Scheme of a molecular orbit of a singlet-state oxygen molecule; (a2) scheme of a molecular orbit of a triplet-state oxygen molecule; (b) energy scheme of different mechanistic pathways for spin-parallel (blue) and spin-antiparallel (red) photogenerated holes (or  $\cdot\text{OH}$  radicals) when water is oxidized to produce oxygen and hydrogen. (c) Scheme of  $\text{H}_2\text{O}_2$  production in the water splitting reaction.

about 10 mA/cm<sup>2</sup>, a lower overpotential, and a much lower yield of H<sub>2</sub>O<sub>2</sub> than the anode coated with achiral NPs does. This finding provides a rational strategy for designing highly active anode material composed of earth-abundant elements by taking advantage of the CISS effect and combining it with NPs.

## ■ ASSOCIATED CONTENT

### Supporting Information

The Supporting Information is available free of charge on the ACS Publications website at DOI: 10.1021/acsenergylett.8b01454.

Reagents, experimental procedures for catalyst synthesis, characterization details, hydrogen evolution, circular dichroism spectra, XPS spectra, and gas chromatography spectra of catalysts (PDF)

## ■ AUTHOR INFORMATION

### Corresponding Author

\*E-mail: ron.naaman@weizmann.ac.il.

### ORCID

Ron Naaman: 0000-0003-1910-366X

### Notes

The authors declare no competing financial interest.

## ■ ACKNOWLEDGMENTS

We acknowledge support from the European Research Council POC-2017, Grant No. 764203-watersplit, from U.S. DOE Grant No. ER46430, the Israel–China program ISF-NSFC Grant No. 2475/17, the National Natural Science Foundation of China (Grant No. 51802130), and Jiangsu Provincial Project for Lifting Young Scientific Researchers (2017).

## ■ REFERENCES

- (1) Gratzel, M. Photoelectrochemical Cells. *Nature* **2001**, *414*, 338–344.
- (2) Voiry, D.; Shin, H. S.; Loh, K. P.; Chhowalla, M. Low-Dimensional Catalysts for Hydrogen Evolution and CO<sub>2</sub> Reduction. *Nat. Rev. Chem.* **2018**, *2*, 0105.
- (3) Hisatomi, T.; Kubota, J.; Domen, K. Recent Advances in Semiconductors for Photocatalytic and Photoelectrochemical Water Splitting. *Chem. Soc. Rev.* **2014**, *43*, 7520–7535.
- (4) Hou, Y. D.; Abrams, B. L.; Vesborg, P. C. K.; Björketun, M. E.; Herbst, K.; Bech, L.; Setti, A. M.; Damsgaard, C. D.; Pedersen, T.; Hansen, O.; et al. Bioinspired Molecular Co-Catalysts Bonded to a Silicon Photocathode for Solar Hydrogen Evolution. *Nat. Mater.* **2011**, *10*, 434–438.
- (5) Anantharaj, S.; Ede, S. R.; Sakthikumar, K.; Karthick, K.; Mishra, S.; Kundu, S. Recent Trends and Perspectives in Electrochemical Water Splitting with an Emphasis on Sulfide, Selenide, and Phosphide Catalysts of Fe, Co, and Ni: A Review. *ACS Catal.* **2016**, *6*, 8069–8097.
- (6) Yu, Y.; Pan, L.; Son, M.; Mayer, M. T.; Zhang, W.; et al. Solution-Processed Cu<sub>2</sub>S Photocathodes for Photoelectrochemical Water Splitting. *ACS Energy Lett.* **2018**, *3*, 760–766.
- (7) Ager, J. W.; Shaner, M. R.; Walczak, K. A.; Sharp, I. D.; Ardo, S. Experimental Demonstrations of Spontaneous, Solar-driven Photoelectrochemical Water Splitting. *Energy Environ. Sci.* **2015**, *8*, 2811–2824.
- (8) Liu, J.; Liu, Y.; Liu, N.; Han, Y.; Zhang, X.; Huang, H.; Lifshitz, Y.; Lee, S.; Zhong, J.; Kang, Z. Metal-Free Efficient Photocatalyst for Stable Visible Water Splitting via a Two-Electron Pathway. *Science* **2015**, *347* (6225), 970–974.
- (9) Liu, J.; Zhang, Y.; Lu, L.; Chen, W.; Wu, G. Self-Regenerated Solar-Driven Photocatalytic Water-Splitting by Urea Derived Graphitic Carbon Nitride with Platinum Nanoparticles. *Chem. Commun.* **2012**, *48*, 8826–8828.
- (10) Seabold, J. A.; Choi, K.-S. Effect of a Cobalt-Based Oxygen Evolution Catalyst on the Stability and the Selectivity of Photo-Oxidation Reactions of a WO<sub>3</sub> Photoanode. *Chem. Mater.* **2011**, *23*, 1105–1112.
- (11) Mtangi, W.; Kiran, V.; Fontanesi, C.; Naaman, R. Role of the Electron Spin Polarization in Water Splitting. *J. Phys. Chem. Lett.* **2015**, *6*, 4916–4922.
- (12) Mtangi, W.; Tassinari, F.; Vankayala, K.; Vargas Jentsch, A.; Adelizzi, B.; Palmans, A. R. A.; Fontanesi, C.; Meijer, E. W.; Naaman, R. Control of Electrons' Spin Eliminates Hydrogen Peroxide Formation During Water Splitting. *J. Am. Chem. Soc.* **2017**, *139*, 2794–2798.
- (13) Mondal, P. C.; Mtangi, W.; Fontanesi, C. Chiro-Spintronics: Spin-Dependent Electrochemistry and Water Splitting Using Chiral Molecular Films. *Small Methods* **2018**, *2*, 1700313.
- (14) Tassinari, F.; Banerjee-ghosh, K.; Parenti, F.; Kiran, V.; Mucci, A.; Naaman, R. Enhanced Hydrogen Production with Chiral Conductive Polymer-Based Electrodes. *J. Phys. Chem. C* **2017**, *121*, 15777–15783.
- (15) Naaman, R.; Waldeck, D. H. The Chiral Induced Spin Selectivity Effect. *J. Phys. Chem. Lett.* **2012**, *3*, 2178–2187.
- (16) Naaman, R.; Waldeck, D. H. Spintronics and Chirality: Spin Selectivity in Electron Transport Through Chiral Molecules. *Annu. Rev. Phys. Chem.* **2015**, *66*, 263–81.
- (17) Michaeli, K.; Kantor-Uriel, N.; Naaman, R.; Waldeck, D. H. The Electron's Spin and Molecular Chirality- How Are They Related and How Do They Affect Life Processes? *Chem. Soc. Rev.* **2016**, *45*, 6478–6487.
- (18) Swierk, J. R.; Méndez-Hernández, D. D.; McCool, N. S.; Liddell, P.; Terazono, Y.; Pahk, I.; Tomlin, J. J.; Oster, N. V.; Moore, T. A.; Moore, A. L.; Gust, D.; Mallouk, T. E. Metal-free Organic Sensitizers for Use in Water-splitting Dye-sensitized Photoelectrochemical Cells. *Proc. Natl. Acad. Sci. U. S. A.* **2015**, *112*, 1681–1686.
- (19) Yun, Q.; Lu, Q.; Zhang, X.; Tan, C.; Zhang, H. Three-Dimensional Architectures Constructed from Transition-Metal Dichalcogenide Nanomaterials for Electrochemical Energy Storage and Conversion. *Angew. Chem., Int. Ed.* **2018**, *57*, 626–646.
- (20) Ovid'ko, I. A.; Valiev, R. Z.; Zhu, Y. T. Review on Superior Strength and Enhanced Ductility of Metallic Nanomaterials. *Prog. Mater. Sci.* **2018**, *94*, 462–540.
- (21) Moloney, M. P.; Gun'ko, Y. K.; Kelly, J. M. Chiral Highly Luminescent CdS Quantum Dots. *Chem. Commun.* **2007**, *0* (38), 3900–3902.
- (22) Zhou, Y.; Yang, M.; Sun, K.; Tang, Z.; Kotov, N. A. Similar Topological Origin of Chiral Centers in Organic and Nanoscale Inorganic Structures: Effect of Stabilizer Chirality on Optical Isomerism and Growth of CdTe Nanocrystals. *J. Am. Chem. Soc.* **2010**, *132* (22), 6006–6013.
- (23) Ma, W.; Xu, L.; de Moura, A. F.; Wu, X.; Kuang, H.; Xu, C.; Kotov, N. A. Chiral Inorganic Nanostructures. *Chem. Rev.* **2017**, *117*, 8041–8093.
- (24) Chen, H.; Zhou, J.; Deng, J. Helical polymer/Fe<sub>3</sub>O<sub>4</sub> NPs Constructing Optically Active, Magnetic Core/shell Microspheres: Preparation by Emulsion Polymerization and Recycling Application in Enantioselective Crystallization. *Polym. Chem.* **2016**, *7*, 125–134.
- (25) Safaei-Ghomi, J.; Zahedi, S. L-Proline-functionalized Fe<sub>3</sub>O<sub>4</sub> Nanoparticles as a Novel Magnetic Chiral Catalyst for the Direct Asymmetric Mannich Reaction. *Appl. Organomet. Chem.* **2015**, *29*, 566–571.
- (26) Bloom, B. P.; Kiran, V.; Varade, V.; Naaman, R.; Waldeck, D. H. Spin Selective Charge Transport through Cysteine Capped CdSe Quantum Dots. *Nano Lett.* **2016**, *16*, 4583–4589.
- (27) Li, Z.; Kong, C.; Lu, G. Visible Photocatalytic Water Splitting and Photocatalytic Two-Electron Oxygen Formation over Cu- and Fe-Doped g-C<sub>3</sub>N<sub>4</sub>. *J. Phys. Chem. C* **2016**, *120* (1), 56–63.

(28) Gu, B.; Kiwi, J.; Graetzel, M. Photochemical water cleavage in Suspensions of Pt-Loaded Titania Particles with 0.7% Overall Light to Chemical Conversion Efficiency. *Hydrogen Systems* **1986**, *1*, 121–134.